POLITECNICO
MILANO 1863

DIPARTIMENTO DI MECCANICA

mecc

Accepted manuscript: Analysis of FOWT dynamics in 2-DOF hybrid HIL wind tunnel experiments

I. Bayati, A. Facchinetti, A. Fontanella, F. Taruffi, M. Belloli

This is a post-peer-review, pre-copyedit version of an article published in Ocean Engineering.
The final authenticated version is available online at:
http://dx.doi.org/10.1016/j.oceaneng.2019.106717

DIPARTIMENTO DI MECCANICA ■ POLITECNICO DI MILANO
via G. La Masa, 1 ■ 20156 Milano ■ EMAIL (PEC): pecmecc@cert.polimi.it
http://www.mecc.polimi.it
Rev. 0

Accepted manuscript: Analysis of FOWT dynamics in 2-DOF hybrid HIL wind tunnel experiments

Published in Ocean Engineering, Volume 195, 1 January 2020, 106717
doi: 10.1016/j.oceaneng.2019.106717

I. Bayati[a,b], A. Facchinetti[a], A. Fontanella[a], F. Taruffi[a], M. Belloli[a]

[a]*Department of Mechanical Engineering, Politecnico di Milano, Via La Masa 1, 20156, Milano, Italy*
[b]*Maritime Research Institute Netherlands (MARIN), Wageningen, Netherlands*

Abstract

This paper presents the main results of experimental hybrid/HIL wind tunnel tests of the National Renewable Energy Laboratory (NREL) 5MW wind turbine coupled with the DeepCwind semi-submersible floating platform. Experiments in still water and in irregular waves without wind are compared to corresponding FAST simulations in order to assess the effectiveness of the proposed HIL methodology and to highlight the main sources of uncertainty. Tests are repeated under three wind conditions, corresponding to different wind turbine operating points, to evaluate the effect of the aerodynamic force field on the overall system response. Experimental results are compared to the output of FAST simulations to investigate its prediction capability with respect to the influence of unsteady aerodynamic loads on the FOWT dynamics.

Keywords: Floating offshore wind turbine, wind tunnel testing, hardware in the loop testing, hybrid testing, model validation, hydrodynamics

1. Introduction

Floating offshore wind turbines (FOWTs) are identified as the key technology to install multi-megawatt wind turbines in deep waters, where the adoption of traditional bottom-fixed solutions is impractical. Servo-aero-hydro-elastic simulation codes were recently developed to support the design and certification of FOWTs and experimental data are of great importance for calibration and validation of these tools. Even if some limitations are present, the use of scale models allows to perform tests under closely controlled environmental conditions, reducing uncertainties and requiring lower costs with respect to full-scale experimentation. These limitations are mainly related to the impossibility of perfectly matching all the relevant physics at reduced scale [1], especially in the case of coupled aerodynamic and hydrodynamic problems that usually require different scaling strategies (i.e. Reynolds and Froude scaling respectively).

Most of the scale model experiments on FOWTs performed so far have been following a traditional approach: the complete floating system is scaled according to Froude similitude and it is tested in an ocean basin with physical generation of wind and waves. An example is the first test campaign performed within the DeepCwind consortium which aim was to compare the experimentally measured response of a tension leg platform [2, 3], a spar [4] and a semi-submersible [5] with the output of FAST [6] simulations. A geometrically-scaled rotor was used and results were biased by the poor aerodynamic performance of the wind turbine scale model. A second experimental campaign was carried out with a performance-scaled rotor (i.e. the blade shape was modified to match the performance of the full-scale machine) [7, 8], but also in that case it resulted difficult to reproduce the expected aerodynamic loads at the low-Reynolds numbers resulting from Froude scaling [9].

Hardware-In-the-Loop (HIL) and Software-In-the-Loop (SIL) testing techniques were recently proposed for solving the Froude-Reynolds conflict, improving the accuracy of scale model tests, making simpler the study of global FOWT dynamics both in ocean basin as well in wind tunnels. In case of HIL/SIL ocean

basin tests, the scale model wind turbine rotor is replaced by a system able to generate equivalent aerodynamic loads. A numerical model of the wind turbine rotor takes as input the measured platform displacements and it is integrated in real-time to determine rotor loads that are then applied to the physical model (force control, motion feedback) by means of tendons [10, 11], a winch system [12], a ducted fan [13, 14] or multifans [15]. A complementary testing technique was recently developed at Politecnico di Milano (PoliMi) [16, 17] in order to investigate global FOWT dynamics taking advantage of the Atmospheric Boundary Layer (ABL) test section of GVPM [18]. A wind turbine physical scale model is used to generate proper aerodynamic/rotor loads. Forces measured at tower-base are combined to numerically computed hydrodynamic loads and are treated as the input of a numerical model of the floating platform and mooring lines [19] that is integrated in real-time. The resulting platform rigid-body displacements are imposed to the wind turbine model (motion control, force feedback).

The PoliMi HIL testing methodology is presented in [20], with particular attention to the measurement of aerodynamic loads and how these are used for real-time integration of the platform model. In that work, the stand-alone numerical model of the floating platform was verified against the FAST v8.16 model of the DeepCwind semi-submersible for no-wind cases only, to identify differences in the platform response due to the approach used for the modeling of platform hydrodynamics. The same set of tests was then repeated on a 2-DOFs HIL setup to assess the robustness of the system to real measurements and non-ideal actuation. In [19], the 2-DOFs platform model at the base of the HIL numerical subsystem was extended to 6-DOFs and a code-to-code assessment versus an equivalent FAST model was performed, discussing the effects of modeling choices imposed by computational constraints.

The DeepCwind 2-DOFs HIL system is also considered in this work. As already mentioned, the numerical model at the base of the HIL system was assessed against FAST v8.16 in [20]. The comparison pointed out that the deviations between the two hydrodynamic models introduce negligible differences

in the platform response. For still air conditions it is then reasonable to ascribe any significative discrepancy between numerical simulations and HIL experiments to the HIL setup itself and, in particular, to the adopted measurement and actuation chains. In order to identify and quantify their effects on the reproduction of platform dynamics, no-wind verification tests were repeated, extending the test matrix already presented in [20]: free-decay tests were performed for a larger number of initial conditions and two additional sea states were considered for wave-only load cases. Still-air experimental results were systematically compared to the outputs of FAST simulations in equivalent environmental conditions. Once the impact of methodological uncertainties was assessed, tests were repeated for three constant wind speeds and the effect of the aerodynamic loads on the FOWT global response was evaluated. The blade pitch controller has a strong impact of the global motion of the floating platform [21, 22] and its implementation is a complex challenge for floating wind energy. In the present test campaign it was however preferred to exclude its action and perform tests fixing the blade pitch angle to limit the complexity of the experiment. Simulations equivalent to HIL tests were run in order to assess the prediction capability of FAST/*AeroDyn 14* with respect to the influence of unsteady aerodynamic loads on the floating platform surge and pitch response.

2. HIL experimental approach

The HIL experimental approach allows to study global FOWT dynamics through wind tunnel tests by dividing the floating system into a physical and a numerical substructures. A general scheme of the HIL methodology developed at PoliMi to perform wind tunnel tests is shown in Figure 1. The physical substructure is represented by the wind turbine scale model, which is designed so as to reproduce realistic rotor-related loads and control actions. The floating structure response, hydrodynamic loads and mooring lines dynamics are simulated by the numerical substructure. Rotor loads are measured at the model tower base and they represent the input of the numerical model. The latter is

integrated in real-time to compute the wind turbine rigid-body motion that is in turn imposed to the scale model by the HIL actuation system.

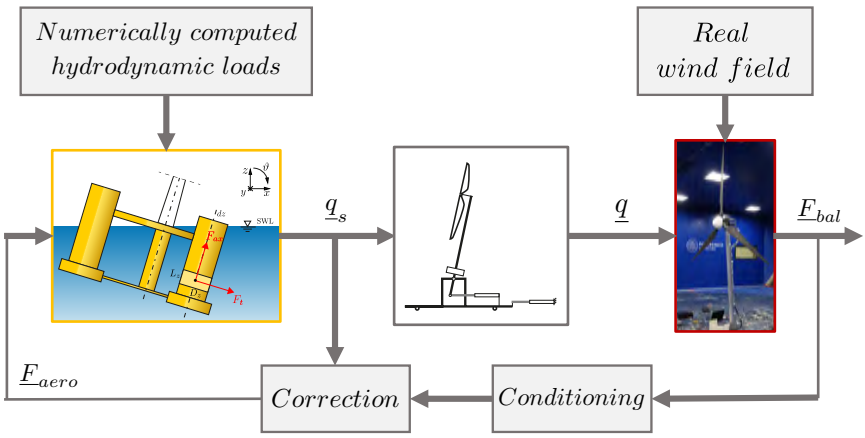

Figure 1: General control scheme of the HIL setup.

The complete analytical formulation at the base of the HIL methodology can be found in [20], however basic equations are recalled here for the sake of clarity. The dynamic response of platform degrees of freedom (DOFs) $\underline{q}$ is expressed by Equation 1. The measured aerodynamic loads $\underline{F}_{aero}$ are combined with numerically computed hydrodynamic loads, mooring line forces, inertial and gravitational loads for real-time integration of the floating system rigid-body equations of motion. Computed platform displacements along surge and pitch DOFs represent the set-point signals given to the respective hydraulic actuators that move accordingly the wind turbine scale model (see Figure 2).

$$[M_s + A_\infty]\,\ddot{\underline{q}} + [R_s]\,\dot{\underline{q}} + [K_s]\,\underline{q} = \underline{F}_{hydro} + \underline{F}_{aero} \tag{1}$$

Vector $\underline{q} = [x\ \theta]^T$ collects the response of surge and pitch coordinates, $\underline{F}_{hydro}$ is the vector of hydrodynamic and mooring lines loads, $[M_s]$ is the 2-by-2 structural mass matrix of the floating system obtained from linearization of the Lagrange term of kinetic energy, $[A_\infty]$ is the infinite frequency added mass matrix, obtained from 3D panel code computations (e.g. WAMIT) under the assumption of potential flow, $[R_s]$ is the linear added damping matrix and $[K_s]$ is the

stiffness matrix, obtained according to Equation 2

$$[K_s] = [K_{hst}] - [K_{grav}] \tag{2}$$

where $[K_{hst}]$ is the hydrostatic stiffness matrix and $[K_{grav}]$ is the gravitational stiffness matrix. Computed hydrodynamic and mooring lines loads, collected in vector $\underline{F}_{hydro}$ are integrated together with aerodynamic loads $\underline{F}_{aero}$. The aerodynamic loads are obtained from Equation 3, subtracting the wind turbine model inertial and gravitational loads (correction forces $\underline{F}_{corr}$) from the overall forces measured by a 6-components load cell at tower base $\underline{F}_{bal}$.

$$\underline{F}_{aero} = \underline{F}_{bal} + \underline{F}_{corr} \tag{3}$$

Correction forces are computed according to Equation 4 from experimentally measured properties (mass matrix $[M_t]$ and gravitational stiffness matrix $[K_t]$) and the simulated platform state $\underline{q}_s$.

$$\underline{F}_{corr} = [M_t]\underline{\ddot{q}_s} + [K_t]\underline{q}_s \tag{4}$$

The main scope of this work is to present the results of the first test campaign performed with the HIL system described above. More details about the methodological approach can be found in [20, 23].

3. Physical and numerical models

Experimental HIL tests presented in this paper are about the DeepCwind floating wind turbine as defined in phase II of OC4 project. The system is composed of the DeepCwind platform and the NREL 5MW baseline wind turbine [24].

3.1. FAST model

A FAST model of the floating system was created to be used as benchmark for no-wind HIL tests. The model reproduces, at full-scale, the 1/50 DeepCwind floating platform scale model used at MARIN for ocean basin experiments [25],

combined to PoliMi wind turbine model. The FAST model was calibrated within OC5 Phase II to match the outputs of experiments for no-wind conditions [26]. In this way it was possible to ensure that the hydrodynamic loads and rigid-body dynamics reproduced by the FAST model were consistent with ocean basin measurements.

3.2. HIL numerical model

A second numerical model of the floating system was developed at PoliMi in *MathWorks Simulink* to be used for real-time integration during HIL tests. The model simulates the hydrodynamic loads due to incoming waves, mooring lines forces and the rigid-body dynamics of the floating system. Rotor loads and aerodynamic forces are not modeled here since, in HIL experiments, their reproduction is demanded to the physical wind turbine scale model. The stand-alone version of the HIL model (i.e. numerical model with numerical inputs) was tuned to match the output of the DeepCwind FAST model for no-wind conditions.

3.3. HIL physical model

As shown in Figure 2 the HIL setup is composed of two hydraulics actuators that move a scaled wind turbine model along the surge and pitch DOFs according to the outputs of the HIL numerical model. The wind turbine mounted on the HIL mechanism is a 1/75 scale model of the DTU 10MW reference wind turbine (RWT) [27], designed and realized by the authors within LIFES50+ project [28, 29]. The DTU 10MW was designed starting from a direct upscale of the NREL 5MW, with the rotor diameter increased of a factor $\sqrt{2}$ in order to gather doubled power. This means that it is possible to consider to PoliMi WTM a $\sqrt{2}/75 \approx 1/53$ scale model of the NREL 5MW.

The PoliMi wind turbine model rotor was specifically designed to operate at the low-Reynolds conditions met during wind tunnel tests [30] through an ad-hoc optimization procedure. The tower first fore-aft mode is at a frequency of 0.36 Hz (at full-scale), above the wind and wave excitation range (rigid tower).

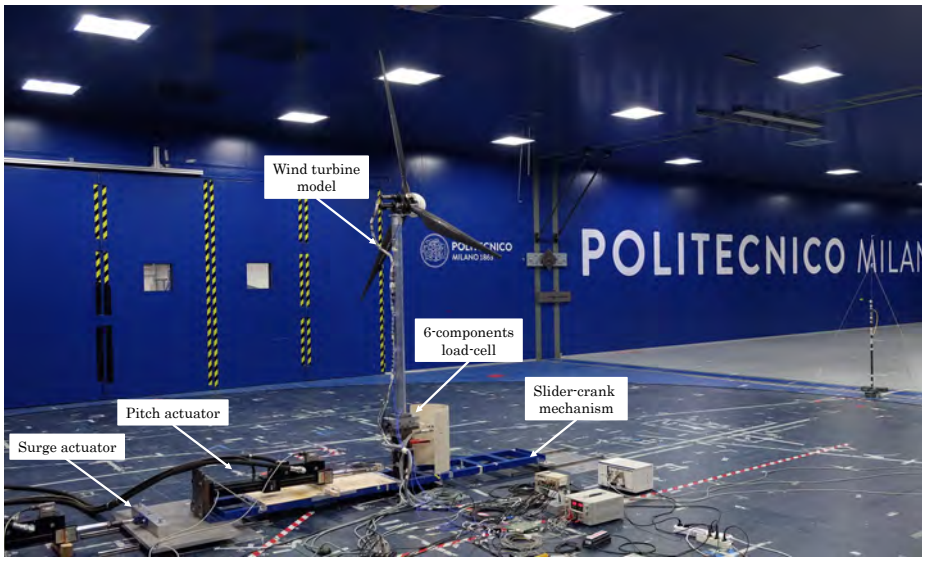

Figure 2: 2 DOFs HIL setup inside the wind tunnel.

Multiple instruments were mounted on the wind turbine model used for HIL experiments and data about rotor position, angular speed, instantaneous torque, effective platform motion, accelerations at multiple tower locations were collected together with tower-top and tower-base forces measured by dynamometric cells.

4. Free-decay tests

The natural frequency and damping of the platform rigid-body motion modes were assessed through free-decay tests. Experiments were performed by imposing to a single platform DOF (either platform surge or platform pitch) a perturbation with respect to the static equilibrium position and allowing the system to move freely. Simulations corresponding to experiments were run in FAST; experimental and numerical data were then processed with the same procedure. For each run, only the response of the directly excited platform DOF was analyzed, disregarding the response induced by coupling on the other platform DOF, considered to be negligible. The natural frequency f_n of the selected

platform rigid-body motion mode was detected from the FFT of the platform DOF response whereas the linear damping coefficient h for the generic platform DOF was derived from the decrease of motion amplitude of the first ten positive peaks in the analyzed decay response.

4.1. Still air

Free-decay tests in still air were performed imposing different initial conditions to the two platform DOFs and repeating the same test with a rotor-collective blade-pitch angle of 0° and 90°. The platform surge and platform pitch free-decay response in still-air are reported in Figure 3 for an imposed initial translation of 5.3 meters with respect to the surge static equilibrium position and a rotor-collective blade-pitch angle of 90°. As visible, an overall good

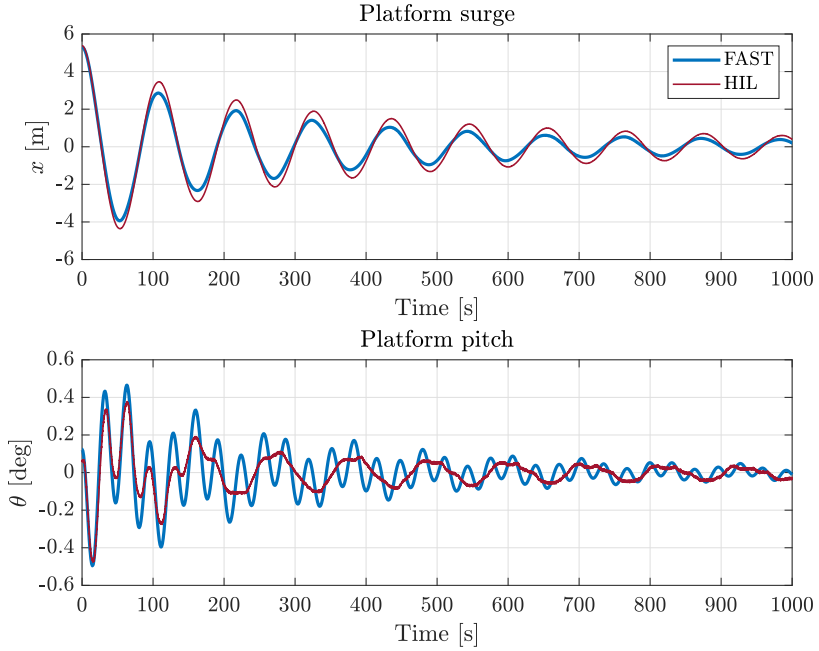

Figure 3: Free-decay test in still air for an imposed platform surge translation of +5.3 meters. Platform surge and platform pitch response.

agreement is obtained between the measured surge response and the target simulation, with the FAST output slightly more damped than the corresponding experiment. A greater difference is seen for the platform pitch response: oscillations at the pitch natural frequency are more damped in HIL experiments than in the corresponding numerical simulations. The platform surge dynamic properties in still-air, resulting from decay tests performed from different initial conditions, are summarized in Table 1.

		FAST		**HIL**	
IC	β	$\mathbf{f_n}$ **[Hz]**	**h [%]**	$\mathbf{f_n}$ **[Hz]**	**h [%]**
-2.9 m	0°	0.009	3.532	0.009	2.763
-5.3 m	0°	0.009	4.092	0.009	2.967
+ 5.3	90°	0.009	4.024	0.009	3.306
-2.9 m	90°	0.009	3.527	0.009	2.663
-5.3 m	90°	0.009	3.994	0.009	2.930

Table 1: Dynamic properties of platform surge mode in still air.

The platform surge and platform pitch free-decay response in still-air are analyzed in Figure 4 for an imposed initial platform pitch rotation of 8° with respect to the static equilibrium position and a rotor-collective blade-pitch angle of 90°. The experimental platform pitch response matches the output of the corresponding FAST simulation quite well, especially in the first cycles. Some differences are seen for the response of the not-directly excited DOF (platform surge), where oscillations at the pitch natural frequency are more damped than in the corresponding simulation. The platform pitch dynamic properties in still-air are compared to the output of corresponding FAST simulations in Table 2.

As shown in Table 1 and 2, the natural frequency of the surge and pitch modes is correctly predicted by the HIL system, regardless of the selected initial condition (IC) and rotor pitch angle. More evident differences are instead present in the floating system damping. The damping for the platform surge

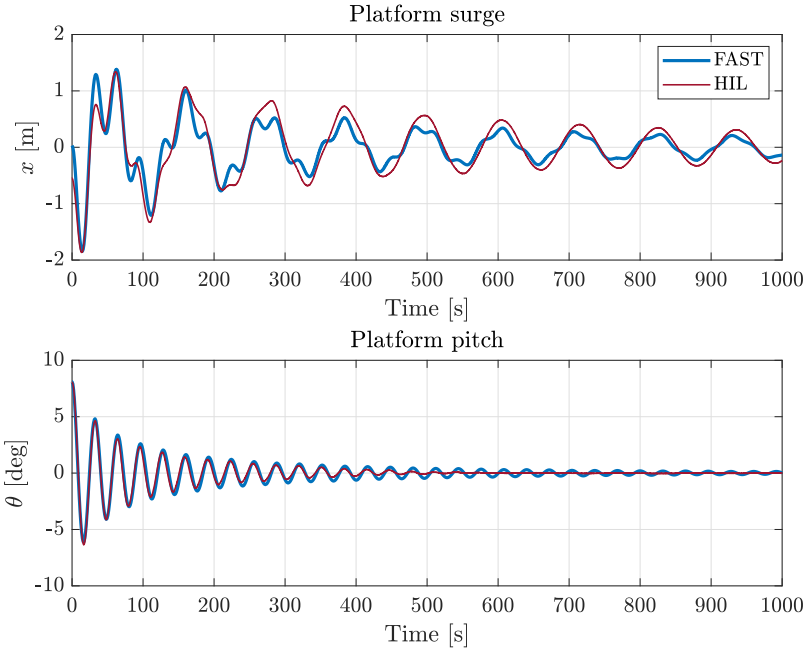

Figure 4: Free-decay test in still air for an imposed platform pitch rotation of +8°. Platform surge and platform pitch response.

mode is lower in HIL tests than in the corresponding FAST simulations. The slight lack of damping could be attributed to a different reproduction of the aerodynamic drag developed by rotor blades when moved in still air. The platform pitch mode damping resulting from HIL experiments is higher than in numerical simulations. This is partially related to the non-negligible dynamics of hydraulic actuators, being the platform pitch actuation less prompt. Moreover, errors in the identification of the wind turbine scale model inertial parameters may result in additional unphysical inertial and gravitational loads on the floating system as discussed in [20, 23] [1]. The combination of a non-compensated gravitational component in the pitch moment measured at tower-base and delays in the mea-

[1] For the sake of conciseness these errors are considered as included in measurement chains uncertainties.

		FAST		HIL	
IC	β	$\mathbf{f_n}$ **[Hz]**	**h [%]**	$\mathbf{f_n}$ **[Hz]**	**h [%]**
+8°	0°	0.031	3.089	0.032	4.472
+4°	0°	0.031	2.467	0.031	4.562
-4°	0°	0.031	2.415	0.032	4.012
-8°	0°	0.031	3.060	0.032	4.137
+8°	90°	0.031	3.100	0.031	4.376
+4°	90°	0.031	2.488	0.032	4.825
-4°	90°	0.031	2.436	0.031	3.875
-8°	90°	0.031	3.068	0.032	4.078

Table 2: Dynamic properties of platform pitch mode in still air.

surement and actuation may affect the platform pitch mode linear damping, as discussed in §3. Differences between experimental and numerical results are more evident for small initial conditions and this could be attributed to non-
195 linearities introduced by the HIL setup.

4.2. Laminar wind

Free-decay tests were also performed for three different laminar wind conditions and the corresponding wind turbine operating points. Any active control
200 logics was used, with rotor speed and pitch angle fixed to the values reported in Table 3, that were chosen to reach the target steady-state thrust force of the NREL 5MW [24].

The platform modes were alternatively excited imposing an initial surge displacement of +5.3 m and a pitch rotation of +8°, and the effect of the aerody-
205 namic force field on the floating system dynamic properties was assessed from the decay response. Natural frequency and linear damping of the considered platform modes were extracted from experimental time records with the same approach as for tests in still air. Experimental results are shown in Figure 5,

Table 3: Wind turbine operating conditions for wind-only tests.

Operating point	U [m/s]	ω_R [rpm]	β [deg]
Below	9.0	10.2	-3.5
Rated	11.4	13,5	-1.0
Above	14.0	13,5	7.2

where are also compared to the output of the corresponding tests in still air (reported in the figure as *No wind*).

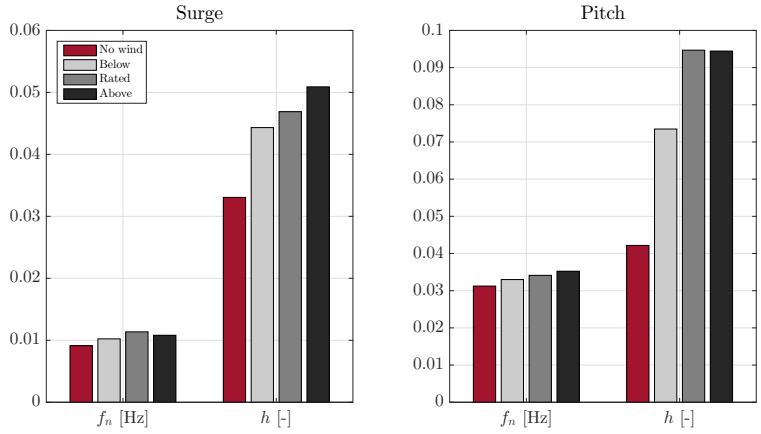

Figure 5: Platform modes dynamic properties for different wind conditions resulting from HIL experiments.

Simulations equivalent to experimental HIL tests were performed in FAST v8, evaluating the natural frequency and damping of the platform surge and pitch DOF from the resulting decay motions. Results for the three wind conditions of Table 3 and still air are reported in Figure 6.

The natural frequency of the surge and pitch platform modes, affected by the positional component of the aerodynamic force field, is almost unchanged by presence of wind. Small differences are seen in HIL experiments for the pitch mode frequency but these are not present in FAST simulations. The platform modes damping is affected by the aerodynamic force field component

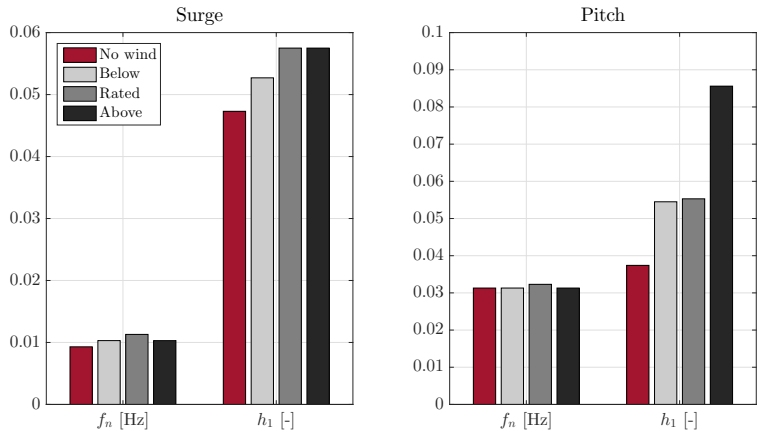

Figure 6: FAST platform modes dynamic properties for different wind conditions resulting from FAST simulations.

proportional to the platform motion rate. Significative variations are highlighted by HIL experiments for both the surge and pitch modes. A damping increment is also predicted by FAST but this is less evident than in HIL experiments. The surge damping is almost constant for increasing wind speeds whereas the pitch mode damping has a significative increment only for the above-rated wind condition.

5. Irregular waves tests

Three irregular wave conditions were considered in order to examine the floating wind turbine response to stochastic hydrodynamic loads. The operational wave already part of OC5 Phase II load cases [26] was complemented with Fos wave, representative of moderate sea conditions [31], and DNV wave for a mild environment simulation [32]. Parameters of the JONSWAP spectrum for the above mentioned wave conditions are resumed in Table 4.

5.1. Methodology

For any HIL tests a wave elevation time series was generated from the JONSWAP spectrum for the assigned significant wave height H_s and peak period T_p

Table 4: Wave conditions for HIL experiments and FAST simulations.

Wave condition	H_s [m]	T_p [s]
Operational	7.10	12.10
Fos	4.00	8.00
DNV	1.86	7.20

and additional energy was introduced in the difference-frequency band to model second order wave kinematics. Memory constraints of the real-time controller that run the HIL model imposed to compute wave loads from wave elevation time series shorter than the test duration. This required to assume wave elevation data periodic for times longer than wave time history.

Referring to Figure 7, in a typical HIL test, wave elevation data are available from time t_3 when acquisition starts. Before t_3, wind and wave loads are separately applied to the floating system and, in between, a wait-time interval is used to let the system reach steady-state conditions. In particular, at t_0, wind and rotor rotation are applied to the wind turbine and forces measured at tower base start to be integrated by the HIL model. At t_1, when the aerodynamics is assumed to be at regime, wave excitation forces are applied to the platform and, at t_2, when the numerical model is again at regime, HIL actuators are enabled and the wind turbine model is moved according to platform displacements calculated in real-time. Acquisition starts when the system is at regime again.

In order to compare experimental and numerical results it was necessary to reproduce wave loads in FAST, consistently with HIL tests. The FAST HydroDyn module allows to use externally generated wave elevation time series from which wave kinematics are derived [33]. Time series must have a length at least equal to the total simulation time. The imported wave elevation time series are assumed to be of first order and long crested. When second order terms are required, these are calculated from the provided wave elevation data, adding extra-energy at the difference frequencies (frequency range from 0 to

0.05 Hz) according to the extended Stokes theory. Wave elevation time histories acquired in HIL tests, before being imported in FAST, were low-pass filtered, zeroing harmonic components in the difference-frequency range (between 0 and 0.05 Hz) to have first order only wave elevation data.

In FAST, aerodynamic forces and wave loads are simultaneously applied to the floating wind turbine and all the model outputs are available from the beginning of the simulation (see Figure 5). The first part of output time histories, corresponding to a pre-simulation time $t_3 - t_2$, is discarded and analyses are performed on effective time series of length $t_{end} - t_3$. Periodicity in the wave

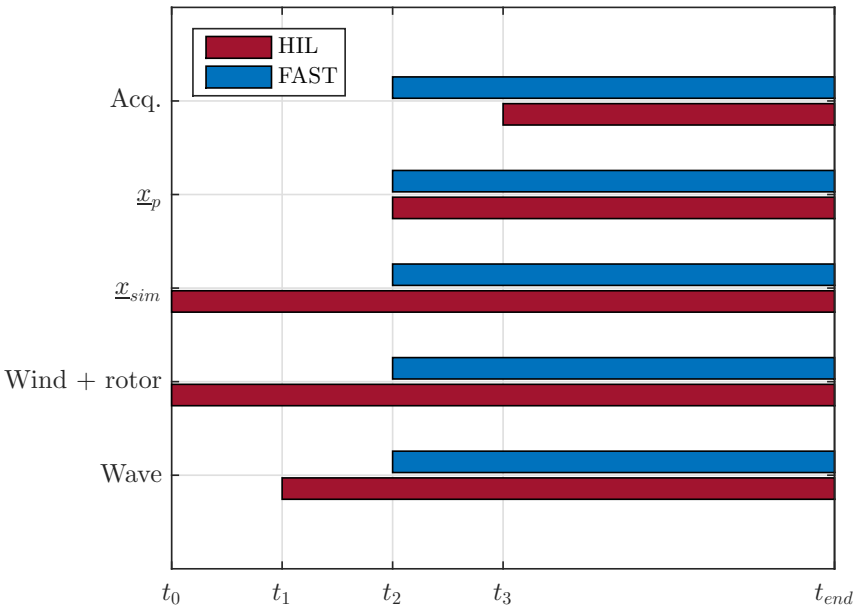

Figure 7: Timing chart for HIL tests and FAST simulations.

elevation time series from HIL tests was identified from autocorrelation analysis. The fundamental wave time history (that was repeated during HIL tests) was extracted and replicated for the number of periods required to cover the pre-simulation time $t_3 - t_2$ and for one period after t_{end}, to ensure a wave elevation time history longer than the total simulation time.

Table 5: Timing chart for HIL tests and FAST simulations.

Time	HIL	FAST
t_0	Wind and rotor rotation	-
t_1	Wave loads	-
t_2	Platform motion	Simulation start
t_3	Acquisition start	-
t_{end}	Acquisition end	Simulation end

The PSD of second-order waves from HIL tests and FAST simulations are compared in Figure 8.

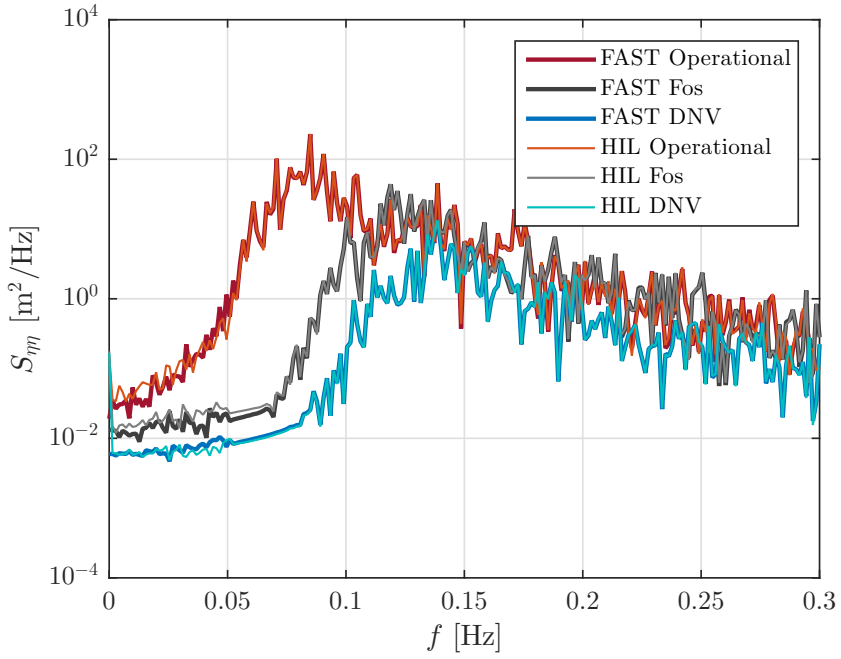

Figure 8: Wave conditions for HIL experiments and FAST simulations.

5.2. Wave-only tests

Wave-only tests were performed to assess the capability of the HIL system

to reproduce the dynamic response of the floating system due to stochastic hydrodynamic loads. The three wave conditions of Table 4 were considered to excite the floating system in the frequency range of interest with variable amplitude wave loads. Low-frequency second-order wave kinematics were included as well as second-order platform forces. FAST simulations were run reproducing wave loads resulting from HIL tests according to the procedure described in §6. The hydraulic actuators used in the experimental setup are featured by a maximum allowed excursion of 250 mm (corresponding to 13.25 m at full-scale) which limits the reproduction of the platform surge when the floater is to a static displacement. For this reason, only the dynamic component was reproduced, discarding the surge static displacement. Similarly, the mean value was subtracted from FAST time series of the surge DOF response.

Time histories of the experimentally measured surge and pitch response are compared to those resulting from the corresponding FAST simulations in Figure 9. Matching between experimental data and numerical computations is very good even if some differences are present. The platform DOFs response to DNV and Fos waves is dominated by harmonic components at frequencies close to the surge mode, whereas in Operational conditions the contribution of the pitch mode is the most significative. The largest response amplitude is recorded, for both the considered DOFs, in Operational conditions, being the wave peak closer to platform rigid-body modes (see Figure 8). The minimum motion amplitude is instead reached for the DNV sea state, that is characterized by low-amplitude waves in the frequency range of platform modes. The amplitude of the low-frequency response recorded in HIL tests is larger than the numerical prediction. This could be related to the lack of damping, already described analyzing decay tests (see Figure 3 and Table 1). A delay is present in any case between the pitch response recorded in HIL tests and the output of FAST simulations. Being wave loads the same for experiments and simulations, the response delay can be related only to the HIL system measurement and actuation chain.

The probability density functions (PDF) estimated from time series of the platform DOFs response are shown in Figure 10. PDFs are useful to under-

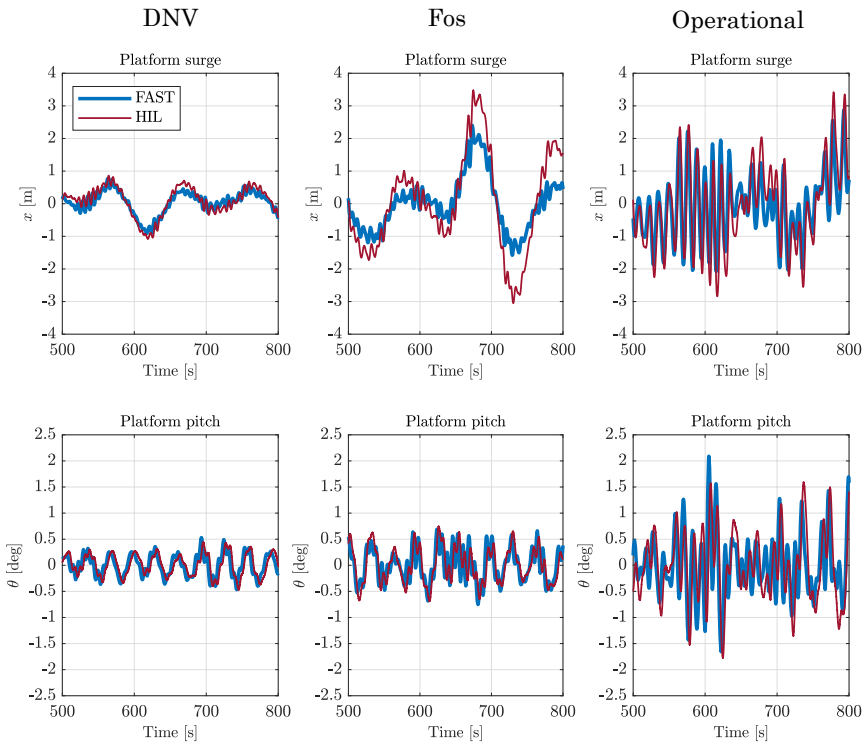

Figure 9: Sample of platform response time histories from HIL tests and FAST simulations for different wave conditions.

stand the distribution of instantaneous values in the platform DOFs response to irregular waves, as well as to evaluate the prediction capability of the HIL system with respect to peak displacements. As visible in Figure 10, a good correspondence is obtained between numerical and experimental PDFs for any wave condition. The PDFs for the platform pitch DOF resulting from the experiments are in good agreement with those obtained from FAST simulations for any of the wave conditions considered here. A good matching is achieved also in the tails of the PDF meaning that the probability of having large displacements in HIL experiments and FAST simulations is very close. A lower correspondence is obtained between the experimental and numerical PDFs for

the platform surge DOF. In this case, the PDF is narrower with larger tails in HIL tests than in the corresponding simulations and this is particularly evident for Fos waves. This behavior can be mainly ascribed to the damping of the platform surge mode that is lower in HIL tests than in FAST simulations (see Table 1).

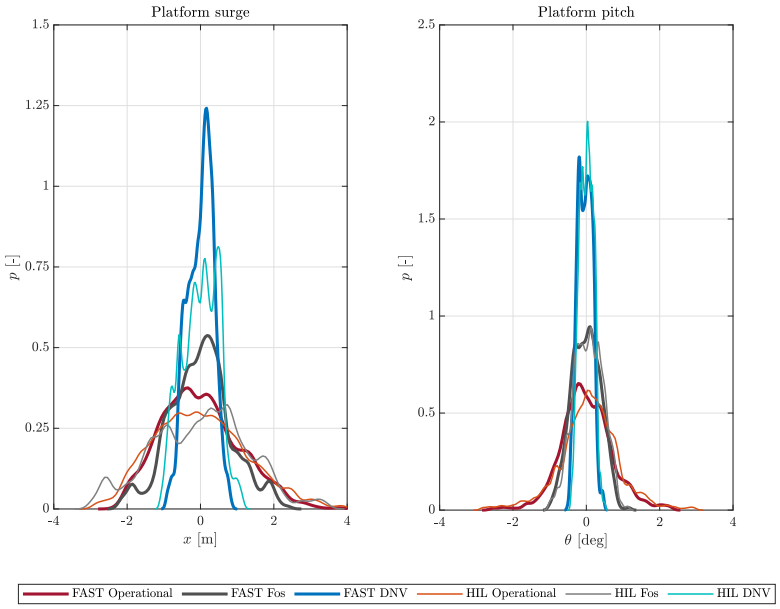

Figure 10: Estimated probability density function (PDF) of platform surge and pitch response from HIL tests and FAST simulations for different wave conditions.

The PSD of the time series presented in Figure 9 are shown in Figure 11 in a frequency range up to 0.3 Hz. The experimental response matches numerical computations for most of the investigated frequencies. The most significative discrepancies are found in the low-frequency range, in correspondence to the platform natural frequencies, where the HIL response is higher than the target. It is worth noticing the pitch response at the pitch mode frequency shows a lower damping in HIL tests than in FAST simulations, contrarily to what was seen in free-decay experiments. This inverse behavior is caused by the additional damping introduced by the non perfect force correction that is different when

the system undergoes a force or free motion.

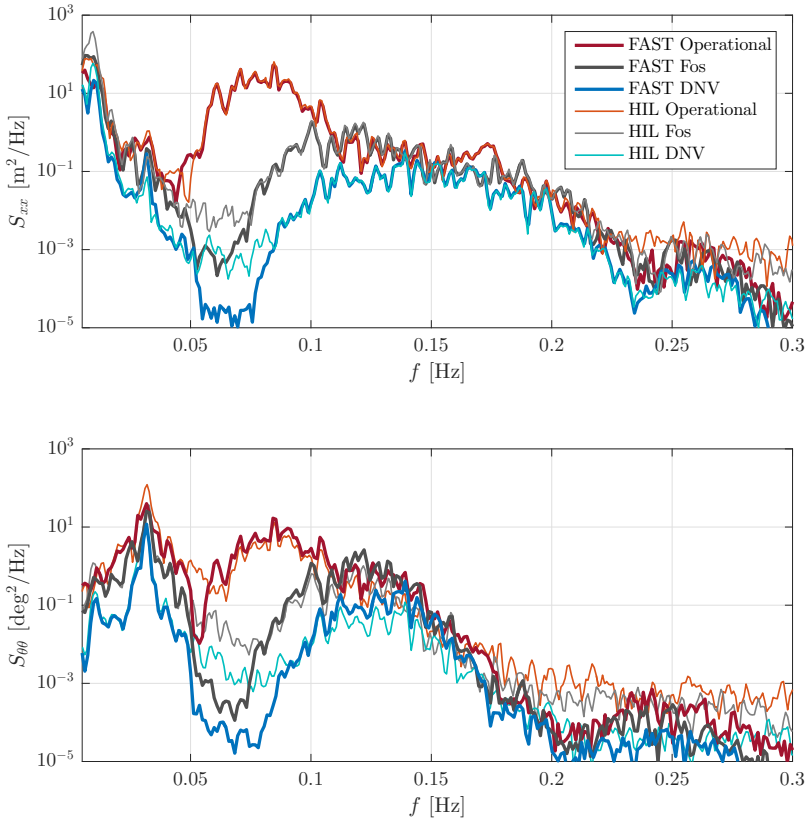

Figure 11: PSD of platform response from HIL tests and FAST simulations for different wave conditions.

Being wave loads the same for the experiment and numerical model, the mismatch between the HIL response and FAST predictions could be also related to additional forcing terms not modeled in FAST, as reported in §3. In Figure 12 the 1st order and 2nd order diffraction forces associated with a wave spectrum of significant wave height H_s of 1.86 m and peak period T_p of 7.2 s (DNV waves) are compared to the HIL residual forces. These are responsible of an additional excitation source, whose effect is more evident in correspondence of the platform

natural frequencies, where energy introduced by waves is lower.

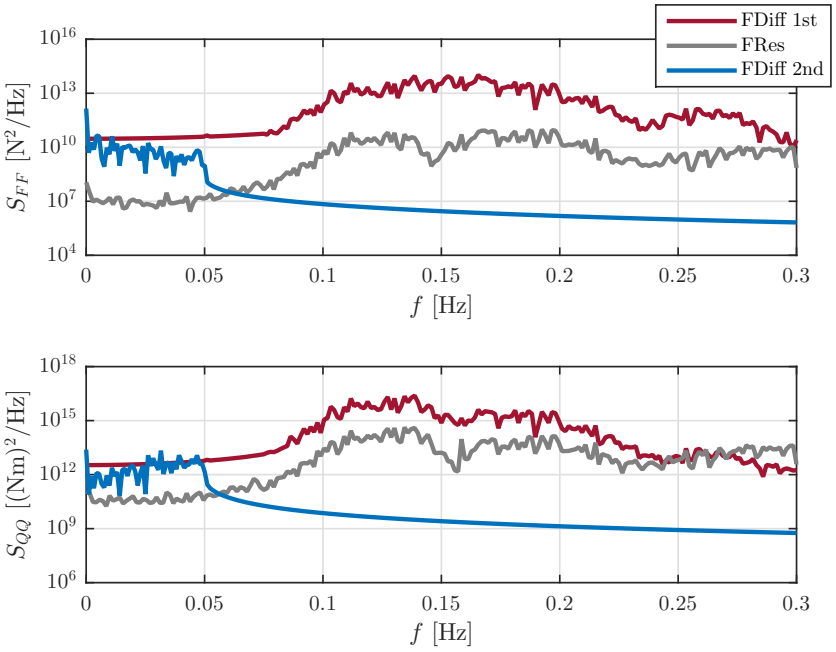

Figure 12: Wave diffraction loads and HIL residual forces for a significant wave height H_s of 1.86 m and peak period T_p of 7.2 s.

Some differences are also shown by the pitch DOF in the linear-wave excitation range (above 0.07 Hz) where the experimental response is lower than target FAST simulations. Figure 13 shows the platform response to DNV waves. The effective surge and pitch motion measured by linear velocity displacement transducers (LVDTs) during HIL experiments is compared to the output of the HIL real-time model (HIL set-point) and the platform response computed with FAST for equivalent environmental conditions. From the PSD, it can be noticed how the set-point given to the HIL pitch actuator matches FAST calculations better than the effective pitch displacement measured by LVDT. The different response in the wave-excitation range could be then related to the actuation system dynamics, that introduces a non-negligible deamplifaction and phase loss in the platform position set-point calculated from integration of the platform

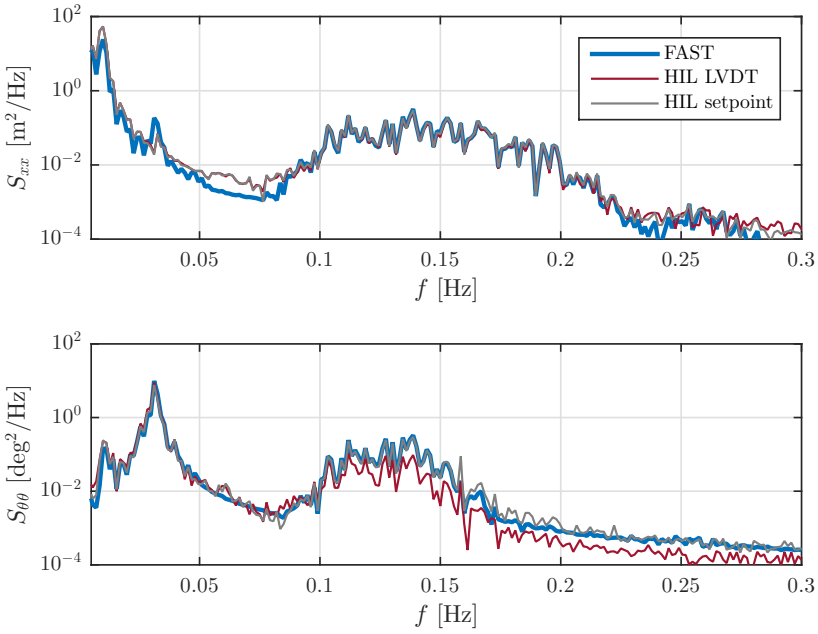

Figure 13: PSD of platform DOFs response for 2nd order wave excitation (significant wave height H_s of 1.86 m and peak period T_p of 7.2 s).

model. It is worth recalling that the observed discrepancies are ascribable to the actuation and measurement chains of the setup , since negligible differences are shown by the comparison between the pure numerical model (i.e. the one adopted for real-time calculations) and FAST model (see §1 and [20]).

5.3. Wind and waves tests

The effect of wind turbine loads on the platform response is investigated for operational waves and the three wind conditions of Table 3. As already mentioned, the rotor speed and the rotor-collective blade-pitch angle were fixed to the values of Table 3 [2] .

[2]The mean percent standard deviation of rotor speed was 0.40% for DNV waves, 0.43% for Fos waves and 0.65% for Operational waves tests.

Operational waves were chosen among the sea states of Table 4 for the significative excitation of the platform modes that makes possible to study the effect of the aerodynamic force field on the FOWT motion. The PSD of the surge and pitch DOFs response measured in HIL tests for operational waves and different wind conditions is shown in Figure 14 whereas the output of the corresponding FAST simulations is reported in Figure 15.

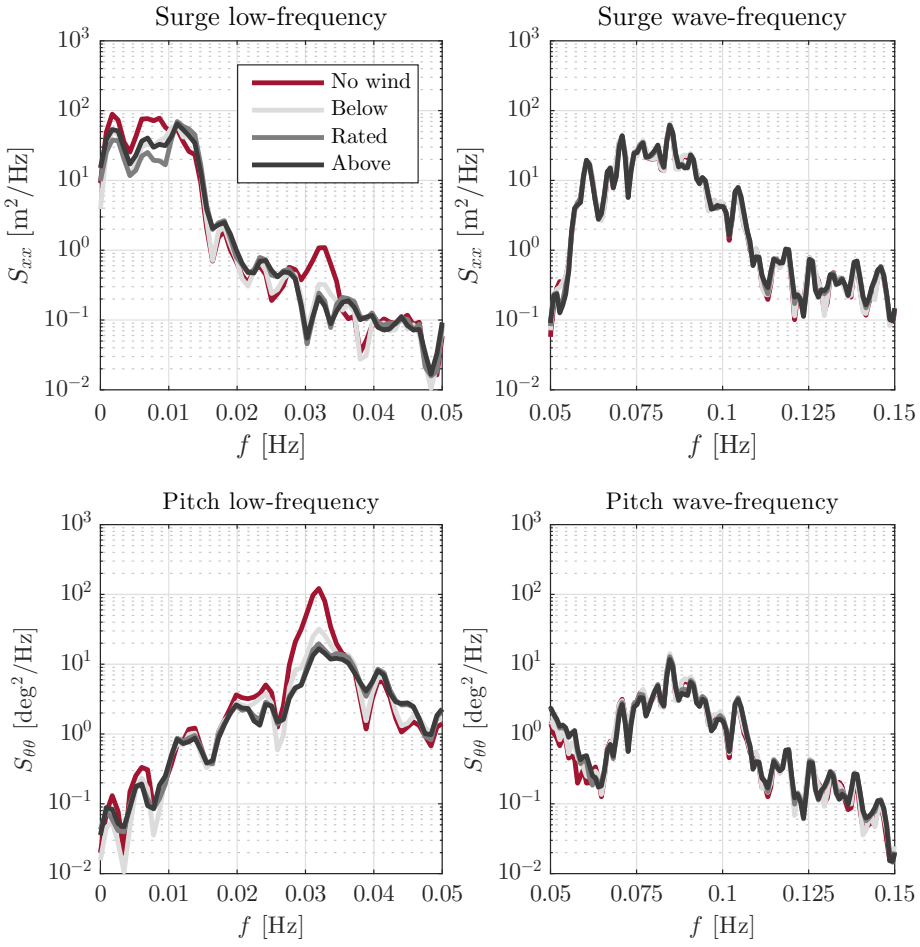

Figure 14: PSD of platform response for operational waves (significant wave height H_s of 7.1 m, peak period T_p of 12.1 s) and different wind conditions resulting from HIL tests.

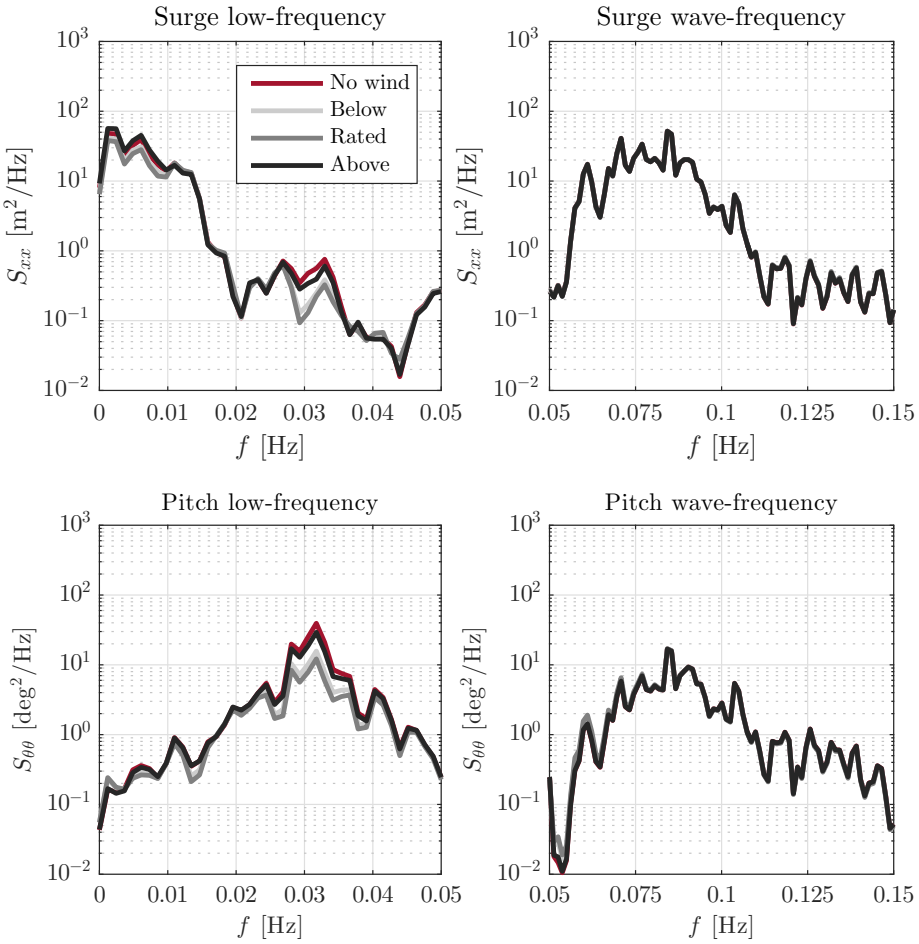

Figure 15: PSD of platform response for operational waves (significant wave height H_s of 7.1 m, peak period T_p of 12.1 s) and different wind conditions resulting from FAST simulations.

The platform motion is analyzed making a distinction between wave-frequency range (0.05 - 0.15 Hz), where the response is governed by linear wave loads, and low-frequency range (0 - 0.05 Hz), where difference-frequency second order wave forces are predominant. In the wave-frequency range, the FOWT response is almost unaffected by the presence of wind and there are no significant differences between the three considered wind turbine operating conditions. A more marked influence of aerodynamic loads on the FOWT response is instead visible in the low-frequency range, in particular in correspondence of the platform

pitch mode. The pitch frequency is almost constant for any operating conditions, whereas the response amplitude is greatly decreased by the presence of wind. This effect is in agreement with the output of free-decay tests that shows a large increment of the pitch mode linear damping for increasing wind speeds.

The irregular wave tests confirm that the aerodynamic loads do not affect the platform natural frequencies, but lead to an increase of the associated damping. Similar findings are reported also in [34], where the DeepCwind motion in surge, pitch and heave to irregular waves (including the effect of second-order loads) was studied for a steady wind of 13 m/s. The same behavior is observed both in HIL experiments and FAST simulation results that show similar predicted response amplitude in presence of wind. However, a larger damping increment is seen in HIL tests than in FAST simulations when passing from a no wind condition to an operating wind turbine.

The cross spectrum density (CSD) of the aerodynamic surge force with the surge motion and the CSD of the aerodynamic pitch moment and pitch motion are computed from HIL data to understand how aerodynamic loads correlates to the platform response in the frequency bands of interest.

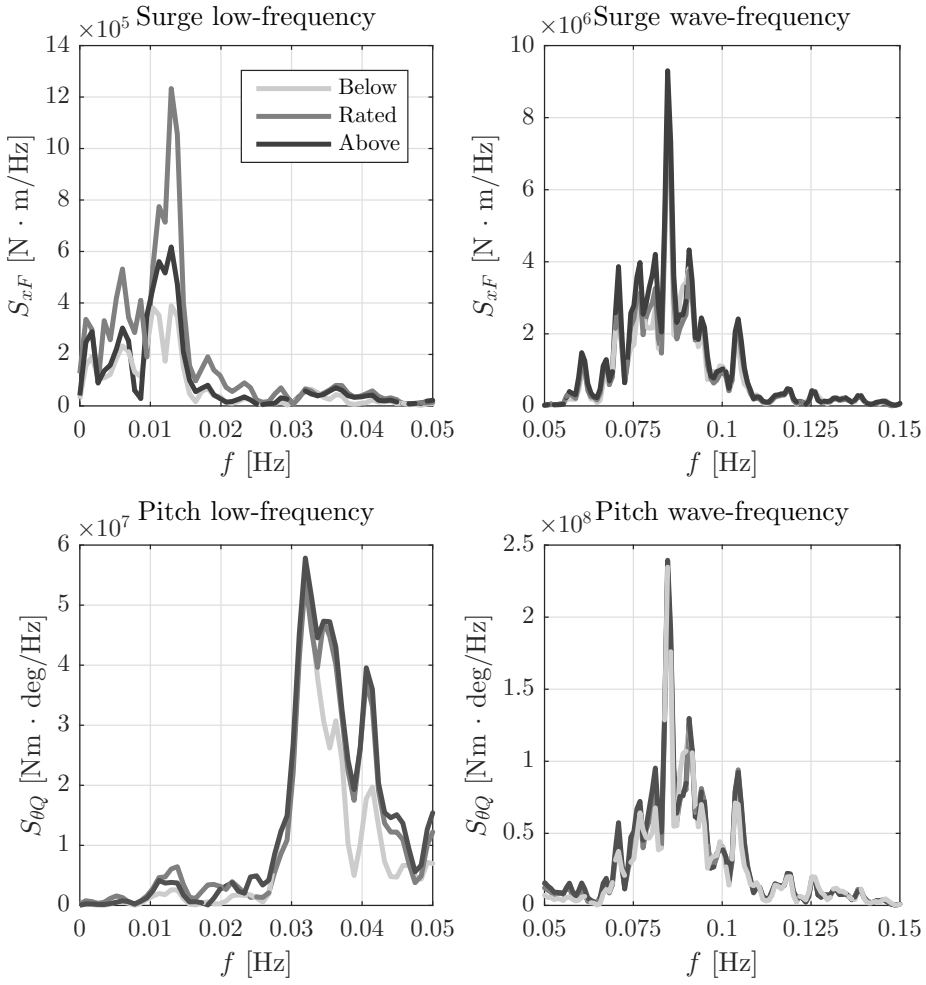

Figure 16: CSD of platform response for operational waves (significant wave height H_s of 7.1 m, peak period T_p of 12.1 s) and different wind conditions resulting from HIL tests.

The CSD relative to the surge DOF is shown in the first row of Figure 16. A narrow peak is found at the surge natural frequency, where the system is excited in resonance, while a broad-band peak is seen in correspondence of the linear-wave excitation range, where the floating platform experiences the largest loads. A similar trend is visible in the CSD of pitch, which is shown in the second row of Figure 16. The interaction with wind is the strongest when the motion of the system is large and significantly affects the effective rotor speed. The

effect of aerodynamic loads is however evident only in correspondence of the floating system natural frequencies, where the response amplitude is strongly modified by the aerodynamic damping, and negligible in the wave-frequency range, where hydrodynamic loads are prevailing. The CSD relative to both the platform DOFs is sensitive to the operating condition only in low-frequency range. The different correlation between loads and platform motion is at the base of the different aerodynamic damping experienced by the system.

6. Conclusions

Hybrid/HIL tests of a semi-submersible floating wind turbine were carried out at the PoliMi wind tunnel. No-wind tests were performed to extensively compare the FOWT behavior as reproduced by the HIL system to the one predicted by equivalent FAST simulations. The main differences are found in the damping of the platform modes, and are introduced by the actuation system and the measurement chain.

Then, the same tests were carried out in still air and under different wind conditions to discuss how the forces developed by the wind turbine rotor affect the floating system global response. It is found that the platform surge and pitch response to irregular waves is different when the turbine is operating or not and the response changes when different operating points are considered. The most significant differences are observable in the low-frequency range, in correspondence of platform modes, on account of the damping introduced by the aerodynamic loads. The difference in the platform response can be attributed to the loads developed by the wind turbine and this is demonstrated by the CSDs of §5.3. A variable correlation between loads and platform motion is seen at the platform resonant frequencies for different wind turbine operating conditions and this translates into a variable damping. FAST analyses were carried out to assess the numerical simulation tool capability of predicting the influence of aerodynamic loads on the floating platform response. The same trends seen in experimental tests are captured by FAST, with more marked differences in the reproduction of the aerodynamic damping introduced by wind turbine loads on

the platform pitch mode.

Wind tunnel tests of the current campaign were carried out at constant rotor speed and rotor-collective blade-pitch angle, excluding the wind turbine control system in order to avoid further uncertainties related to the controller settings. However, recent tests including the action of the wind turbine controller are being carried out to directly investigate how traditional pitch-to-feather control strategies affects the FOWT response [35, 36].

7. Acknowledgements

This project has partially received funding from the European Union Horizon 2020 research and innovation program under grant agreement No 640741. The authors want also to acknowledge master and PhD students who gave their help to the activity over the years: Marco Villa, Davide Bertinat, Simone Ambrosini and Luca Bernini.

References

References

[1] C. L. Bottasso, F. Campagnolo, V. Petrovic, Wind tunnel testing of scaled wind turbine models: Beyond aerodynamics, Journal of Wind Engineering and Industrial Aerodynamics 127 (2014) 11–28. doi:10.1016/j.jweia.2014.01.009.

[2] G. Stewart, M. Lackner, A. Robertson, A. Jonkman, A. Goupee, Calibration and validation of FAST floating wind turbine model of the DeepCwind scaled tension-leg platform, 22nd International Offshore and polar Engineering Conference (ISOPE) - Rhodes, Greece.

[3] B. Koo, A. Goupee, K. Lambrakos, H.-J. Lim, Model test correlation study for a floating wind turbine on a tension leg platform, 32nd International Conference on Ocean, Offshore and Arctic Engineering (OMAE) - Nantes, Francedoi:10.1115/OMAE2013-11590.

[4] J. R. Browning, J. Jonkman, A. Robertson, A. Goupee, Calibration and validation of a spar-type floating offshore wind turbine model using the FAST dynamic simulation tool, Journal of Physics: Conference Series 555 (2014) 012015. doi:10.1088/1742-6596/555/1/012015.

[5] B. Koo, A. Goupee, K. Lambrakos, H.-J. Lim, Model test data correlations with fully coupled hull/mooring analysis for a floating wind turbine on a semi-submersible platform, 33rd International Conference on Ocean, Offshore and Arctic Engineering (OMAE) - San Francisco, CA, USA 9B. doi:10.1115/OMAE2014-24254.

[6] J. M. Jonkman, M. L. Buhl, Fast user's guide, Technical Report NREL/EL-500-38230.

[7] A. Goupee, M. Fowler, R. Kimball, J. Helder, E. J. Ridder, Additional wind/wave basin testing of the DeepCwind semisubmersible with a performance-matched wind turbine, 33rd International Conference on Ocean, Offshore and Arctic Engineering (OMAE) - San Francisco, CA, USA 9B. doi:10.1115/OMAE2014-24172.

[8] R. Kimball, A. J. Goupee, M. J. Fowler, E. J. Ridder, J. Helder, Wind/wave basin verification of a performance-matched scale-model wind turbine on a floating offshore wind turbine platform, 33rd International Conference on Ocean, Offshore and Arctic Engineering (OMAE) - San Francisco, CA, USA 9B. doi:10.1115/OMAE2014-24166.

[9] A. N. Robertson, J. M. Jonkman, M. D. Masciola, P. Molta, A. j. Goupee, C. A. J., I. Prowell, J. Browning, Summary of conclusions and recommendations drawn from the DeepCwind scaled floating offshore wind system tests campaing, 32nd International Conference on Ocean, Offshore and Arctic Engineering (OMAE) - Nantes, France 8. doi:10.1115/OMAE2013-10817.

[10] T. Sauder, V. Chabaud, M. Thys, E. E. Bachynski, L. O. Sæther, Real-time hybrid model testing of a braceless semi-submersible wind turbine.

part I: the hybrid approach, 35th International Conference on Offshore Mechanics and Arctic Engineering (OMAE) - Busan, Korea 6 (49972). doi:10.1115/OMAE2016-54435.

[11] E. E. Bachynski, M. Thys, T. Sauder, V. Chabaud, L. O. Sæther, Real-time hybrid model testing of a braceless semi-submersible wind turbine. part II: Experimental results, 35th International Conference on Offshore Mechanics and Arctic Engineering (OMAE) - Busan, Korea 6 (49972). doi:10.1115/OMAE2016-54437.

[12] S. Gueydon, R. Lindeboom, W. van Kampen, E.-J. de Ridder, Comparison of two wind turbine loading emulation techniques based on tests of a TLP-FOWT in combined wind, waves and current, ASME 2018 1st International Offshore Wind Technical Conference (IOWTC) - San Francisco, CA, USAdoi:10.1115/IOWTC2018-1068.

[13] J. Azcona, F. Bouchotrouch, M. Gonzalez, J. Garciandia, X. Munduate, F. Kelberlau, T. A. Nygaard, Aerodynamic thrust modelling in wave tank tests of offshore floating wind turbines using a ducted fan, Journal of Physics: Conference Series 524 (1) (2014) 012089.

[14] F. Vittori, F. Bouchotrouch, F. Lemmer, J. Azcona, Hybrid scaled testing of a 5MW floating wind turbine using the SiL method compared with numerical models, 37th International Conference on Offshore Mechanics and Arctic Engineering (OMAE) - Madrid, Spain 10. doi:10.1115/OMAE2018-77853.

[15] T. Battistella, D. De Los Dolores Paradinas, A. Meseguer Urban, R. Guanche Garcia, High fidelity simulation of multi-MW rotor aerodynamics by using a multifan, 37th International Conference on Offshore Mechanics and Arctic Engineering (OMAE) - Madrid, Spain 10 (51319). doi:10.1115/OMAE2018-77606.

[16] I. Bayati, A. Facchinetti, A. Fontanella, H. Giberti, M. Belloli, A wind

tunnel/HIL setup for integrated tests of floating offshore wind turbines, Journal of Physics: Conference Series 1037 (5) (2018) 052025.

[17] I. Bayati, M. Belloli, A. Facchinetti, H. Giberti, A 6DOF/HIL setup for wind tunnel hybrid tests on a 1/75 scale model of a 10 MW floating wind turbine, 23rd Conference of the Italian Association of Theoretical and Applied Mechanics (AIMETA) - Salerno, Italy.

[18] Galleria del vento politecnico di milano.
URL http://www.windtunnel.polimi.it

[19] I. Bayati, M. Facchinetti, A. Fontanella, M. Belloli, 6-DoF hydrodynamic modelling for wind tunnel hybrid/HIL tests of FOWT: the real-time challenge, 37th International Conference on Offshore Mechanics and Arctic Engineering (OMAE) - Madrid, Spain 10 (51319). doi:10.1115/OMAE2018-77804.

[20] I. Bayati, M. Belloli, A. Facchinetti, Wind tunnel 2-DOF hybrid/HIL tests on the OC5 floating offshore wind turbine, 36th International Conference on Offshore Mechanics and Arctic Engineering (OMAE) - Trondheim, Norway 10 (57786). doi:10.1115/OMAE2017-61763.

[21] J. M. Jonkman, Dynamics modeling and loads analysis of an offshore floating wind turbine.

[22] T. J. Larsen, T. D. Hanson, A method to avoid negative damped low frequent tower vibrations for a floating, pitch controlled wind turbine, Journal of Physics: Conference Series 75 (2007) 012073. doi:10.1088/1742-6596/75/1/012073.

[23] S. Ambrosini, I. Bayati, M. Facchinetti, M. Belloli, Methodological and technical aspects of a 2DoF/HIL setup for wind tunnel tunnel tests of floating systems, Journal of Dynamic Systems, Measurement, and Control, **forthcoming**.

[24] J. Jonkman, S. Butterfield, W. Musial, , G. Scott, Definition of a 5-MW reference wind turbine for offshore system development, Technical Report NREL/TP-500-38060.

[25] A. Robertson, J. Jonkman, F. Wendt, A. Goupee, H. Dagher, Definition of the OC5 DeepCwind semisubmersible floating system, Technical Report NREL/TP-5000-60601.

[26] A. N. Robertson, F. Wendt, J. M. Jonkman, W. Popko, H. Dagher, S. Guyedon, OC5 project phase II: Validation of global loads of the DeepCwind floating semisubmersible wind turbine, Energy Procedia 137 (2017) 38 – 57. doi:10.1016/j.egypro.2017.10.333.

[27] C. Bak, F. Zahle, R. Bitsche, K. Taeseong, A. Yde, L. C. Henriksen, M. H. Hansen, J. P. A. A. Jose, M. Gaunaa, A. Nataraja, The dtu 10-mw reference wind turbine, DTU Wind Energy Report.

[28] I. Bayati, B. M., L. Bernini, A. Zasso, Scale model technology for floating offshore wind turbines, IET Renewable Power Generationdoi:10.1049/iet-rpg.2016.0956IETDigitalLibrary.

[29] I. Bayati, M. Belloli, L. Bernini, E. Fiore, H. Giberti, A. Zasso, On the functional design of the DTU 10MW wind turbine scale model of LIFES50+ project, Journal of Physics Conference Series 753 (2). doi:10.1088/1742-6596/753/5/052018.

[30] I. Bayati, M. Belloli, L. Bernini, A. Zasso, Aerodynamic design methodology for wind tunnel tests of wind turbine rotors, Journal of Wind Engineering and Industrial Aerodynamics 167 (2017) 217 – 227. doi:10.1016/j.jweia.2017.05.004.

[31] Oceanographic and meteorological conditions for the design, LIFES50+ Deliverable 1.1.

[32] Environmental conditions and environmental loads, Recommended Practice DNV-RP-C205.

[33] J. M. Jonkman, A. N. Robertson, G. J. Hayman, Hydrodyn user's guide and theory manual, Technical Report NREL - Draft.

[34] S. Gueydon, Aerodynamic damping on a semisubmersible floating foundation for wind turbines, Energy Procedia 94 (2016) 367 – 378. doi:10.1016/j.egypro.2016.09.196.

[35] A. Fontanella, I. Bayati, M. Belloli, Linear coupled model for floating wind turbine control, Wind Engineering 42 (2) (2018) 115 – 127. doi:10.1177/0309524X18756970.

[36] A. Fontanella, I. Bayati, M. Belloli, Control of floating offshore wind turbines: Reduced-order modeling and real-time implementation for wind tunnel tests, 37th International Conference on Offshore Mechanics and Arctic Engineering (OMAE) - Madrid, Spain 10 (51319). doi:10.1115/OMAE2018-77840.